sustainability

MDPI

Article

Moisture, Temperature, and Salinity of a Typical Desert Plant (*Haloxylon ammodendron*) in an Arid Oasis of Northwest China

Li Zhao [1,2], Wanjing Li [1,2], Guang Yang [1,2,3,*], Ke Yan [1,2], Xinlin He [1,2,*], Fadong Li [4,5], Yongli Gao [3] and Lijun Tian [4]

1 College of Water and Architectural Engineering, Shihezi University, Shihezi 832000, China; zhaoli_shzu@163.com (L.Z.); 13795665928@163.com (W.L.); keziwell@163.com (K.Y.)
2 Xinjiang Production and Construction Group Key Laboratory of Modern Water-Saving Irrigation, Shihezi 832000, China
3 Center for Water Research, Department of Geological Sciences, University of Texas at San Antonio, San Antonio, TX 78249, USA; yongli.gao@utsa.edu
4 Institute of Geographic Sciences and Natural Resources Research, Chinese Academy of Sciences, University of Chinese Academy of Sciences, Beijing 100049, China; lifadong@igsnrr.ac.cn (F.L.); tianlj87@foxmail.com (L.T.)
5 College of Resource and Environment, University of Chinese Academy of Sciences, Beijing 100049, China
* Correspondence: mikeyork@163.com (G.Y.); hexinlin2002@163.com (X.H.); Tel.: +86-150-0993-0733 (G.Y.)

Abstract: The physical and chemical characteristics of soil and water sources affect desert plants' growth, which is essential for the ecological protection in arid areas. The typical patch patterns of *Haloxylon ammodendron* in the oasis-desert ecotone in the southern margin of the Manas River Basin consists of bare patches (BP) and vegetation patches (VP). The water sources of *H. ammodendron* were studied using stable isotope technology, and the soil physical and chemical properties were monitored and analyzed. The results showed that the soil moisture presented a reversed "S" type curve, and the total salt content of the soil presented an "S" type curve. A "wet island" and "cold island" were formed in the low salt area with *H. ammodendron* at the center. NaCl was most abundant in the BP soil, and the milligram equivalent of Cl^- was 80–90%, while $CaSO_4$ was most abundant in the VP soil, in which the milligram equivalent of SO_4^{2-} was 80–100%. Before the rain, *H. ammodendron* mainly relied on the soil water from a deeper layer (≥60 cm) to maintain its growth. However, after the rain, *H. ammodendron* mainly relied on shallow soil water (<60 cm) to maintain its growth.

Keywords: hydrogeology; desert soils; water resources; Xinjiang China

Citation: Zhao, L.; Li, W.; Yang, G.; Yan, K.; He, X.; Li, F.; Gao, Y.; Tian, L. Moisture, Temperature, and Salinity of a Typical Desert Plant (*Haloxylon ammodendron*) in an Arid Oasis of Northwest China. *Sustainability* **2021**, *13*, 1908. https://doi.org/10.3390/su13041908

Academic Editor: Luca Di Palma
Received: 28 December 2020
Accepted: 3 February 2021
Published: 11 February 2021

1. Introduction

Patch vegetation is composed of discontinuous bare patch (BP) and vegetation patch (VP) [1], which is a typical pattern of vegetation landscape in arid and semi-arid regions [2]. As an important part of the ecosystem in arid areas, natural vegetation is the most intuitive reflection of the natural environment [3]. It is of great significance in controlling the desertification process and protecting biodiversity [4]. Vegetation patch patterns result from the interactions between ecological and hydrological processes in arid areas and are common and relatively stable vegetation forms in arid areas [5]. Patch vegetation is distributed in arid areas worldwide [6]. The Junggar Basin is located in the arid inland area of Northwest China adjacent to the Gurbantunggut Desert, the second largest desert in China [7]. In this area, precipitation is scarce, evaporation is strong, and the ecological environment is fragile.There are many patches and strips of natural vegetation or coppice dune in the Oasis-Desert ecotone [8], forming a patch landscape pattern with *H. ammodendron* as the primary desert vegetation [9,10]. Growth and development of this vegetation mainly depend on atmospheric precipitation or local underground infiltration water [11], and the vegetation coverage is relatively low, generally at 10–30%. It is particularly essential to maintain the ecosystem's stability in arid areas [12]. Since the 1990s, with climate warming

and the aggravation of human activities [13], patch vegetation in arid and semi-arid areas of the world face severe degradation to varying degrees [14].

Water resources may be the leading ecological factors that affect vegetation growth and distribution patterns in arid desert areas. To a certain extent, they control patch vegetation's composition and structure [15]. Also, soil moisture determines the hydrothermal balance of the entire ecosystem and the soil's physical and chemical characteristics, which affect the distribution patterns of vegetation to some extent in arid and semi-arid regions [16,17]. The water sources for plants vary under different climatic and environmental conditions [18,19]. In arid areas, plants can only use surface soil water when there is adequate rainfall [20]. In the dry season with little rain, due to the low water content in the soil, the water is not easily absorbed by the plants, so the plants mainly absorb and utilize the deeper soil water through the deep primary root system [4]. In arid areas, limited by precipitation and a deficiency of available moisture in the soil, the feedback coupling system between water and vegetation closely connects ecological and hydrological processes [21,22]. The coupling of water cycles and patch patterns is the critical factor in maintaining the stable succession of arid desert ecosystems [23]. Quantitative studies on the capture, maintenance, transmission, and redistribution of water and other resources by different vegetation patterns can provide a critical research approach to evaluate the response mechanism of ecosystem changes to the water cycle [24]. Soil moisture determines the whole ecosystem's water and heat balance [21]. In arid and semi-arid areas, soil moisture determines soil properties and the distribution of soil water, salt, and nutrients, which affect the distribution pattern of vegetation to a certain extent [25,26].

In three arid Mediterranean ecosystems in Spain, Greece and Morocco, Kéfi et al. found that the patch-size distribution of the vegetation follows a power law. They propose that patch-size distributions may be a warning signal for the onset of desertification [27]. For a variety of patchy semiarid vegetation types in Australia, Europe, and North America, Ludwig et al. found that patches significantly stored more soil water, produced more growth and had better infiltrability than interpatches [28]. Luo et al. described Spatio-temporal changes in population characteristics in two shrub populations in the transition zone between oasis and desert in the Heihe River Basin, northwestern China, and concluded that summer precipitation was a key factor that affected population characteristics and spatial patterns [29]. Xu et al. studied two typical desert shrub species, *Tamarix ramosissima* and *H. ammodendron*, co-occurring in the Gurbantonggut Desert (Central Asia). For *T. ramosissima*, the primary water resource was groundwater and vadose zone water. For *H. ammodendron*, the primary water resource was precipitation input [30]. In China, due to the high proportion of industrial water and agricultural water, and the low proportion of the ecological water, the carrying capacity of ecological environment in arid areas is reduced, the patch vegetation is seriously degraded, and the problem of land desertification is prominent, which makes the ecological environment construction one of the important problems to be solved urgently in arid areas of China [31]. *H. ammodendron*, as typical vegetation of patch pattern, is one of the most widely distributed desert plants in Central Asia desert area, with strong drought resistance, wind erosion resistance, sand burial resistance and other physiological characteristics [32]. The research on the adaptability of *H. ammodendron* in the arid environment can provide the basis for the restoration and reconstruction of artificial ecology and the sustainable development of oasis in the arid area. Plant stable isotopes are gradually becoming more widely used in ecological research in recent years. Hydrogen and oxygen stable isotopes can be used to study the water use sources of plants quantitatively and then reveal the selective absorption, water sources, and trends of plants exposed to different sources of water [33]. Stable isotope technology has been widely used in the quantitative study of plant water usage [34]. After the plant roots absorb the water, the hydrogen and oxygen isotopes in the stem xylem do not fractionate, and the components remain steady, which is consistent with the stable isotopes in the original water source. In a previous study, stable isotope mixing models were utilized to determine the proportional contributions of various water sources [35]. The

overexploitation and utilization of water resources cause the groundwater depth in arid areas to drop sharply, which leads to local degradation of patch vegetation and aggravation of soil desertification. It is particularly important to study the formation, evolution, and spatial patterns of patch vegetation in arid regions. The survival and coverage rates of *H. ammodendron* directly determine the stability of the patch pattern; therefore, this study focused on the adaptive evaluation of *H. ammodendron*.

To assess the adaptability and water resources utilization for typical desert plant (*H. ammodendron*), a two-year experiment was conducted to compare the soil moisture, temperature, salinity and soil ions between the VP and BP in Manas River Basin, and the stable isotope technology was utilized to determine the water sources. In the experiment, the differences in soil physical and chemical properties between VP and BP were compared. The growth adaptability of *H. ammodendron* was obtained, and the results are significant can provide the basis for ecological conservation in arid areas.

2. Materials and Methods

2.1. Site Description

The experimental zone was located in the oasis-desert ecotone of the Manas River Basin (45°16′53″ N, 86°15′58″ E), where the annual rainfall is 100 mm, annual evaporation is 1000 mm–1500 mm, soil type is sandy loam, and the vegetation coverage rate is only approximately 30% (Figure 1). The annual average temperature is 10.0 °C, and the extreme maximum and minimum temperatures are 38.1 °C and −25.1 °C, respectively (Figure 2). There is a massive temperature difference between day and night in winter and summer. The annual sunshine duration is 2777 h, the accumulated temperature is 3594 °C, and wind primarily occurs in the spring and summer seasons, with a maximum wind speed of 20 m/s. The groundwater is at an approximate depth of 13 m. There are abundant sand plants and drought-resistant plants in this area. *H. ammodendron* is the dominant vegetation type.

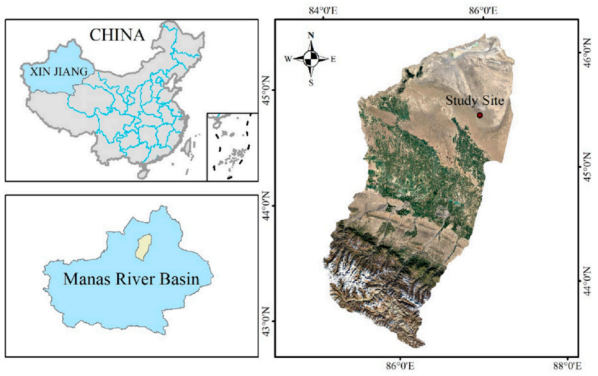

Figure 1. Location of the experimental field (45°16′ N, 86°15′ E) in the Manas River Basin.

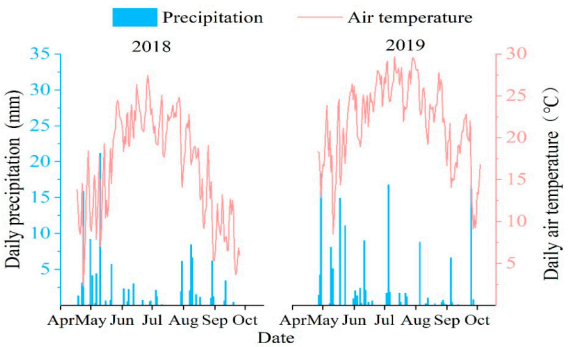

Figure 2. Daily air temperature (red line) and daily precipitation (blue bars) in 2018 and 2019.

2.2. Experimental Design

2.2.1. Soil Water Content and Soil Salinity

The soil profile was divided into five sampling intervals (0–30, 30–60, 60–90, 90–120, 120–150, and 150–180 cm) for the soil water content, temperature, and salinity measurements (Figure 3). Soil samples were collected from May to October in 2018 and 2019 at a depth of 0–180 cm from the VP of *H. ammodendron* and soil BP. An ENVI data-DT probe system (ENVI data-DT 1000 series; Beijing Yugen Technology Co., Ltd., Beijing, China) was used to monitor the soil water, temperature, and salinity, with a measurement accuracy of 0.01 m^3/m^3 for moisture, 0.1 °C for temperature, and 10 us/cm for salinity. Samples were taken every 30 cm to determine the soil pH, salinity, and ion concentrations. Meteorological factors are measured by a small automatic weather station (Product model: HOBO H21-USB; Origin: Cape Cod, Massachusetts, USA). The measurement indexes include rainfall (mm) and atmospheric temperature (°C). The measurement frequency is 30 min.

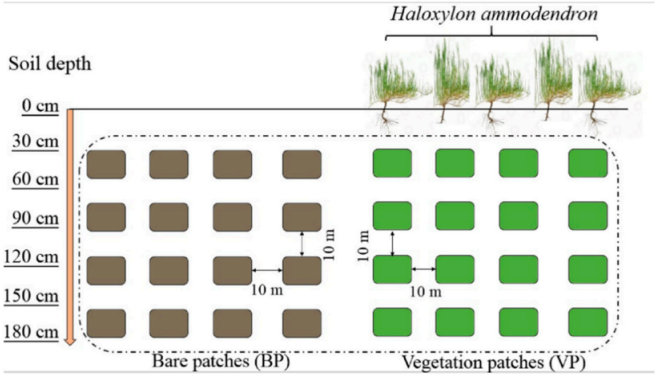

Figure 3. Layout of the experimental plots to measure soil moisture, temperature, salinity, and hydrochemical ions.

2.2.2. Hydrochemical Ions

The HCO_3^- and CO_3^{2-} contents were determined by a double indicator-neutralization titration [36], Cl^- content was determined by silver nitrate titration [37], SO_4^{2-} content was determined by EDTA indirect complexometric titration [38], Ca^{2+} and Mg^{2+} contents were determined by EDTA titration [39], Na^+ and K^+ contents were determined by flame photometry [40], soil pH was determined by potentiometry using an acidity meter, a glass electrode, and a pH composite electrode [41], and soil moisture was determined by the oven drying method. The above measurements were repeated three times, and the average values were obtained.

2.2.3. Water Stable Isotope Measurement

The hydrogen and oxygen isotope compositions ($\delta^{18}O$ and δD) in the soil water, groundwater, and plant water were measured using an LGR IWA-45EP water-vapor isotope analyzer (LGR IWA-45EP; LICA United Technology Limited, Beijing, China) in the Key Laboratory of Modern Water-Saving Irrigation of Xinjiang Production and Construction Group. The results were reported in conformity to the standard Vienna Standard Mean Ocean Water (VSMOW). The measurement precisions for $\delta^{18}O$ and δD were 0.1% and 0.4%, respectively. The following equations gave $\delta^{18}O$ and δD:

$$\delta^{18}O = [(^{18}O/^{16}O)_{Sample} - (^{18}O/^{16}O)_{VSMOW}]/(^{18}O/^{16}O)_{VSMOW} \times 10^3‰ \quad (1)$$

$$\delta D = [(D/H)_{Sample} - (D/H)_{VSMOW}]/(D/H)_{VSMOW} \times 10^3‰ \quad (2)$$

Deuterium excess (d), a second-order parameter which combines both oxygen and hydrogen isotopic species, is defined by the following expression:

$$d = \delta D - 8 \times \delta^{18}O\ 10^3‰ \quad (3)$$

Water was extracted from the soil samples and branches of *H. ammodendron* using an LI-2000 liquid water extractor (LI-2000 liquid water extractor; LICA United Technology Limited, Beijing, China). The water samples were sealed in 50 mL glass bottles, capped with no headspace, sealed with parafilm, and stored in a refrigerator for future water isotope analyses.We used a two-tracer for the three-component model to calculate the mixing ratio based on the following equations:

$$F_A + F_B + F_C = 1 \quad (4)$$

$$\delta^{18}O_A\ F_A + \delta^{18}O_B\ F_B + \delta^{18}O_C\ F_C = \delta^{18}O_{Sample} \quad (5)$$

$$d_A\ F_A + d_B\ F_B + d_C\ F_C = d_{Sample} \quad (6)$$

The water balance calculation utilized the iso-error dual-isotope three-source model described by Phillips and Gregg [42]. This mixing model calculates the estimates and confidence intervals of a source's proportional contributions to a mixture using stable isotope analyses. For dual-isotope studies, the measurements of the two isotope signatures for the samples from the mixture population and the three source populations should be independent of each other.

3. Results

3.1. Soil Temperature

A decrease in the soil temperature with a corresponding increase in BP and VP soil depth was observed. It was most likely due to the high temperatures and sizeable solar radiation in August, which significantly increased the surface temperature (°C) (Figures 4 and 5).

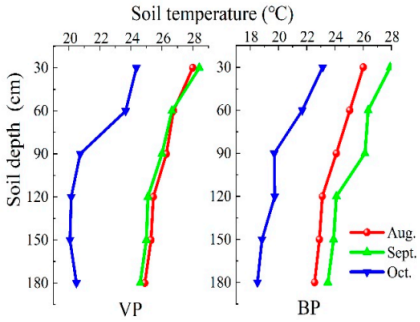

Figure 4. Soil temperature at different depths in VP and BP.

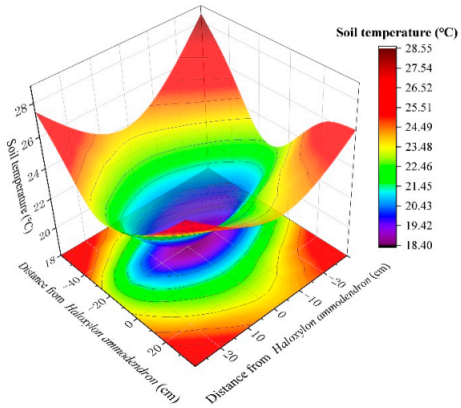

Figure 5. "Cold island effect" map.

When the soil depth was 30–120 cm, the soil temperature decreased obviously with the increase in depth; the soil temperature decreased from 28 °C at a depth of 30 cm to

26 °C at a depth of 120 cm in August, from 28 °C to 25.5 °C in September, and from 24 °C to 20 °C in October. The most significant temperature difference was as high as 4 °C. When the soil depth was 120–180 cm, there was a slight change in the deeper layer's temperature until it became stable.

Vegetation covers weaken solar radiation and illumination, which causes VP to have lower-temperature centers than those of BP. The distribution characteristics of gradually increasing the temperature along with VP to BP form a "cold island effect" centered on VP.

3.2. Soil Moisture

The soil moisture content was obtained in the different soil layers with *H. ammodendron* as the center. The soil moisture content of both VP and BP presented a reversed "S" type curve with an increase in soil depth (Figures 6 and 7).

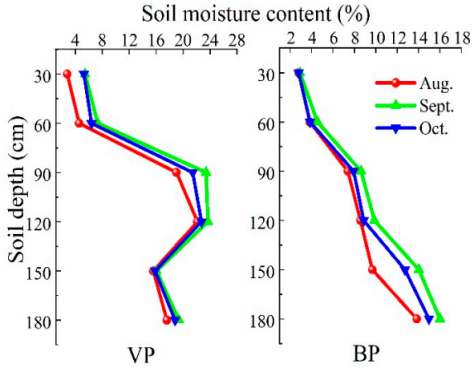

Figure 6. Soil moisture content at different depths in VP and BP.

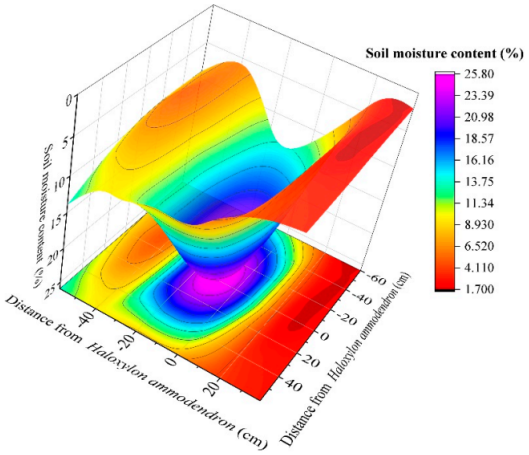

Figure 7. "Wet island effect" map.

The surface soil moisture content of VP was low at 2.8% at 30 cm. With the increase in soil depth to 120 cm, the soil moisture content gradually increased to 22.12%. The soil moisture content of patches in bare soil gradually increased with increased soil depth, from 2.8% at 30 cm and then gradually increasing to 13.83% at 180 cm. On VP, the growth and coverage of *H. ammodendron* reduced evaporation, and the root system of *H. ammodendron* was mainly concentrated in the 50–120 cm soil layer. The soil moisture content in VP was significantly higher than that in BP as the root system absorbed water for plant growth. The highest moisture content was detected in *H. ammodendron*, which gradually decreased to the periphery, forming a "wet island" centered on the *H. ammodendron* plant.

3.3. Soil Salinity

The soil salinity of VP and BP showed an "S" type curve (Figures 8 and 9).

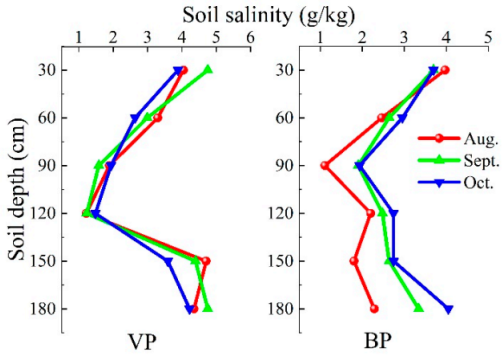

Figure 8. Spatial and temporal distribution of soil salinity at different depths of VP and BP.

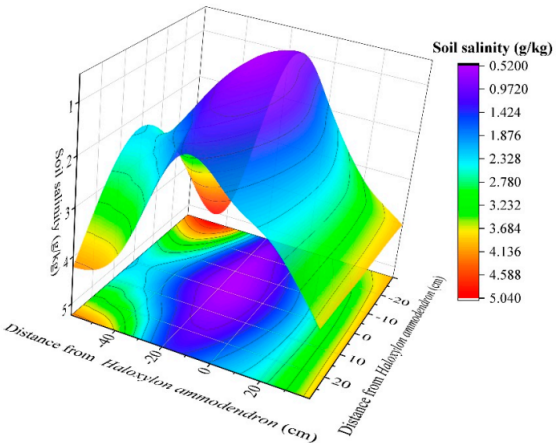

Figure 9. Low salinity area centred on *H. ammodendron*.

The high salinity at the soil surface was due to groundwater evaporation with the high desert temperature, which caused salinity accumulation on the soil surface. The soil salt content of VP was much lower than that of BP, with *H. ammodendron* as the lowest point. A low salinity area centered on *H. ammodendron* was formed; this phenomenon suggested that *H. ammodendron* plants' root system has an individual storage capacity for groundwater. It is a salt-tolerant plant. White crystal precipitation occurred on the leaf surface. The root system of *H. ammodendron* absorbs water for its own growth while inhaling the soluble salt in the soil, and finally precipitates from the leaves, which can appropriately reduce the soil salt content, so that the salt content of the soil where *H. ammodendron* grows is lower than that of the surrounding BP. VP is the lowest point and gradually increase in the surrounding area, forming a "low-salt effect" centered on *H. ammodendron*. At the same time, due to strong solar radiation, the BP is not covered by vegetation, and the surface soil water is lost faster than VP. The soil salt in the BP moves from the deep layer to the surface of the soil in a large amount, resulting in a higher soil salt content in the BP. The content near the root system of *H. ammodendron* is lower than that in the surrounding BP.

3.4. Soil Major Ions

The main anions in the soil are SO_4^{2-} and Cl^-, which was consistent with the anions observed in the VP and BP soil (Figure 10).

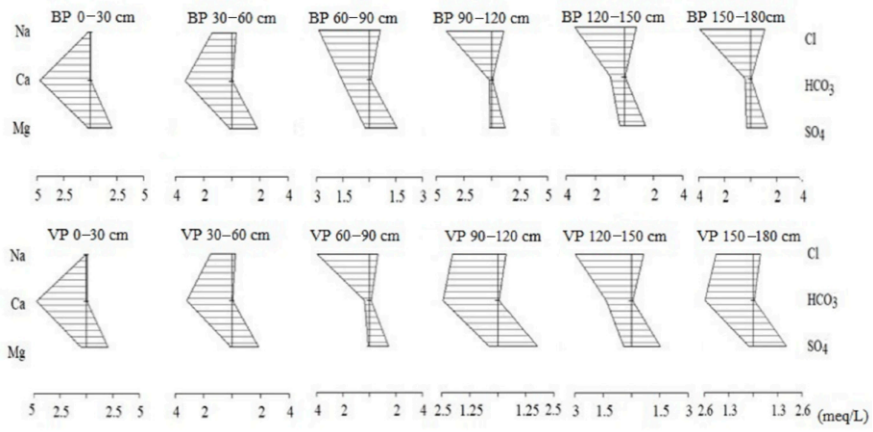

Figure 10. Major ion concentrations (0–180 cm soil depth) under BP and VP.

A decrease and then an increase in the SO_4^{2-} content with an increase in the soil depth was observed. However, Cl^- increased gradually with an increase in the soil depth. The distribution characteristics of SO_4^{2-} showed apparent shallow set surface aggregation, and Cl^- moved deeper into the soil. The main cations in the soil were Ca^{2+} and Na^+. Ca^{2+} first decreased and then increased with an increase in soil depth, which showed distinct distribution characteristics of shallow set surface aggregation. The migration of Na^+ gradually increased with the increase in soil depth due to the soil colloid's effect on Na^+. The contents of K^+ in the cation and Mg^{2+} in the anion were the lowest, and the HCO_3^- content remained the same. The soil salts observed in the oasis-desert ecotone in the Manas River Basin's southern margin were mainly calcium sulfate, sodium sulfate, and sodium chloride.

According to the Piper map, the general hydrochemical types of BP were as follows: SO_4^{2-}-Ca^{2+} was predominant at the surface soil, in which the milligram equivalent of SO_4^{2-} was 80–100%, and the milligram equivalent of Ca^{2+} was 60–90%; with the increase in soil depth, this gradually changed to SO_4^{2-}-Na^+·Ca^{2+}, of which the milligram equivalent of Na^+ was 60–90% (Figure 11). In deep soil, most exist in the form of SO_4^{2-}·Cl^--Na^+. The milligram equivalent of Cl^- was 80–90%. The general hydrochemical types of VP gradually changed from SO_4^{2-}-Ca^{2+} to SO_4^{2-}-Ca^{2+}·Na^+, in which the milligram equivalents of SO_4^{2-}, Ca^{2+}, and Na^+ were 80–100%, 60–90%, and 30–60%, respectively. In deep soil, SO_4^{2-}-Na^+·Ca^{2+} was the most prevalent, and the milligram equivalent of Na^+ was 60–90%.

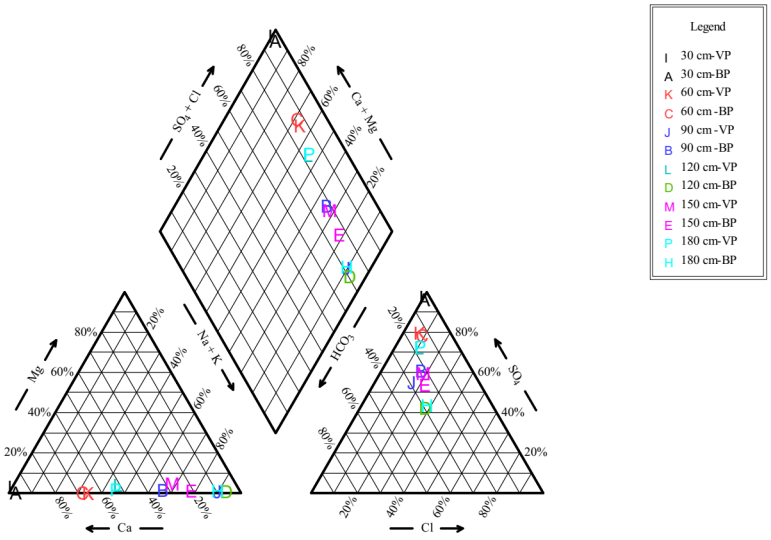

Figure 11. Piper map of soil depth.

3.5. Water Source of H. ammodendron

To measure the difference between the water sources of *H. ammodendron* under two different conditions, i.e., before and after rain, three representative rainy days; namely, 15 July, 23 August, and 16 September 2018, were selected, with rainfalls of 10.0, 12.3, and 8.6 mm, respectively (Figure 12). Before the rain, the values of ^{18}O and D showed that the primary water use source of *H. ammodendron* was groundwater, with an average contribution rate of 37.13%. The second water use source was soil water of the 120–180 cm soil layer, with an average contribution rate of 29.73%, and the 60–120 cm soil layer, with an average contribution rate of 21.38%; and the water use rate of *H. ammodendron* for the shallow soil at 0–60 cm was relatively low, with an average contribution rate of 11.76%. The above data show that *H. ammodendron* utilised the deep soil water and groundwater to a greater extent.

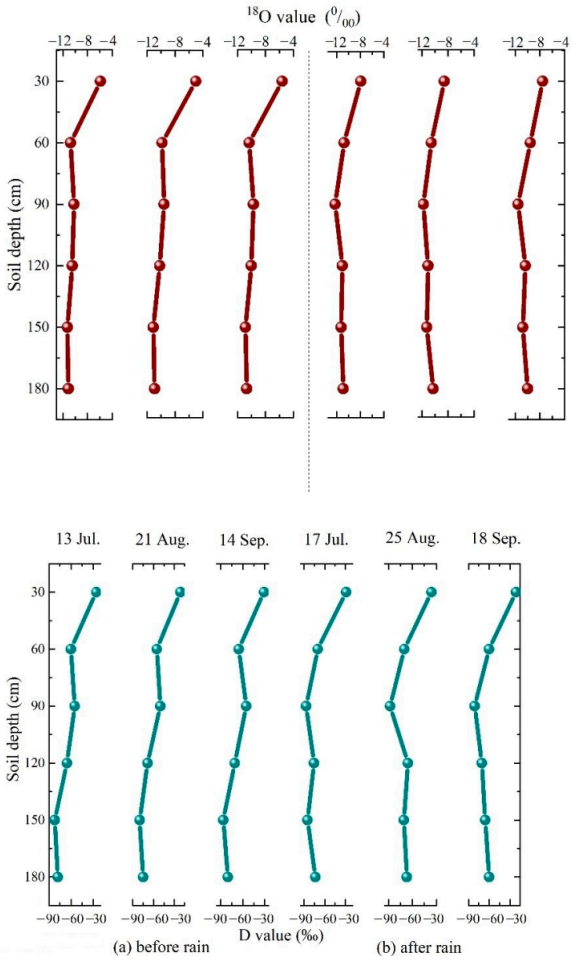

Figure 12. $\delta^{18}O$ and δD values of water at different soil depths.

As shown in Figure 12, the soil should be divided into two layers: 0–60 cm, which may be affected by evapotranspiration, and 60–120 cm, which is relatively stable. According to the isotope measurement from Section 2.2, each potential water source's relative contributions are listed in Tables 1–3.

Table 1. The relative contributions of potential water sources to *H. ammodendron* (15 July).

	Water Source	$\delta^{18}O$	δD	Relative Contribution Rate (%)
Before the rain	Soil water (0–60 cm)	−4.62	0.05	13.52
	Soil water (60–120 cm)	−7.68	0.12	23.47
	Soil water (120–180 cm)	−10.21	0.14	28.87
	Groundwater (Below 180 cm)	−11.67	0.15	34.14
After the rain	Soil water (0–60 cm)	−12.83	0.15	39.93
	Soil water (60–120 cm)	−9.64	0.08	25.17
	Soil water (120–180 cm)	−4.93	0.05	14.27
	Groundwater (Below 180 cm)	−7.12	0.06	20.63

Table 2. The relative contributions of potential water sources to *H. ammodendron* (23 August).

	Water Source	$\delta^{18}O$	δD	Relative Contribution Rate (%)
Before the rain	Soil water (0–60 cm)	−4.98	0.05	13.24
	Soil water (60–120 cm)	−7.96	0.12	22.71
	Soil water (120–180 cm)	−10.19	0.12	30.51
	Groundwater (Below 180 cm)	−11.83	0.14	33.54
After the rain	Soil water (0–60 cm)	−11.96	0.12	39.95
	Soil water (60–120 cm)	−11.86	0.12	25.47
	Soil water (120–180 cm)	−3.42	0.05	13.25
	Groundwater (Below 180 cm)	−10.96	0.08	21.33

Table 3. The relative contributions of potential water sources to *H. ammodendron* (16 September).

	Water Source	$\delta^{18}O$	δD	Relative Contribution Rate (%)
Before the rain	Soil water (0–60 cm)	−4.57	0.05	8.53
	Soil water (60–120 cm)	−9.74	0.06	17.96
	Soil water (120–180 cm)	−10.12	0.08	29.80
	Groundwater (Below 180 cm)	−11.59	0.12	43.71
After the rain	Soil water (0–60 cm)	−12.21	0.13	41.5
	Soil water (60–120 cm)	−11.62	0.07	24.67
	Soil water (120–180 cm)	−8.53	0.05	13.16
	Groundwater (Below 180 cm)	−10.01	0.08	20.67

Groundwater was the primary water source for *H. ammodendron* before the rain, with contribution proportions of 34.14% on 15 July, 33.54% on 23 August, and 43.71% on 16 September. This was followed by the 120–180 cm soil layer, with average contribution proportions of 28.87% on 15 July, 30.51% on 23 August, and 29.80% on 16 September. The 0–60 cm soil layer was the primary water source for *H. ammodendron* after the rain, with contribution proportions of 39.93% on 15 July, 39.95% on 23 August, and 41.50% on 16 September. This was followed by 60–120 cm, with contribution proportions of 25.17% on 15 July, 25.47% on 23 August, and 24.67% on 16 September.

In the case of extensive evaporation of soil water before the rain, *H. ammodendron* mainly relied on the central root system to absorb the groundwater and soil water from a deeper layer (≥60 cm) to maintain its growth. However, after the rain, the utilisation rate of *H. ammodendron* for shallow soil water (<60 cm) increased significantly because the small amount of precipitation could not infiltrate into the groundwater in a short time.

4. Discussion

4.1. Distribution Characteristics of Soil Temperature, Moisture, and Salinity

The soil temperature of bare land patches and vegetation patches decreased with an increase in soil depth. This was due to the high temperatures in August and the sizeable solar radiation; the surface temperature is greatly affected by the environment, so the surface temperature was on the high side [43]. With the increase in soil depth, the effect of environmental factors on soil becomes smaller and smaller, so the temperature of deeper soil changes slightly until it is stable (Figure 13). Vegetation coverage will weaken the solar radiation and light, making the vegetation patches the low-temperature center due to environmental factors, and the bare land patches the high-temperature center [6]. The distribution characteristics of gradually increasing temperature along the vegetation patches to the bare land patches form the "cold island effect" centered on the vegetation patches. The effect of soil temperature also affects the temperature of the air above the vegetation patch, which weakens turbulence development, inhibits the transpiration of plants and evaporation from the ground, and is conducive to vegetation growth [44]. Compared with the vegetation patches in the bare land patches, soil temperature change with soil depth was generally the same. However, the vegetation patches' overall soil temperature was low due to vegetation coverage [45], forming a "cold island effect" centered on *H. ammodendron* vegetation.

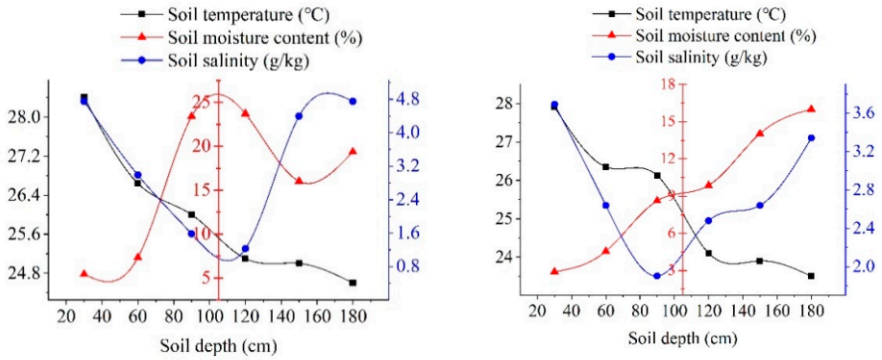

Figure 13. Relationship among the soil temperature, moisture content, and salinity at different soil depths (September) for (**a**) VP and (**b**) BP.

With the increase in soil depth, the vegetation patches' soil moisture content presented an apparent "s" type distribution, that is, the change rule of first increasing, then decreasing, and then increasing again. The vegetation patch's soil water content was significantly higher than that of the bare land patch, which shows that water is a fundamental cause of patch patterns [21]. The surface soil moisture content was the smallest in the vegetation patch and bare land patch, caused by the increase in desert evaporation caused by the high temperature in September (Figure 13). With the increase in soil depth, the influence of temperature on water content gradually decreased, and the water content of VP and BP increased in deep soil [46] (Figure 13). The dry sand layer can block the loss of deep soil water, which is conducive to preserving infiltration water [4,32].

Furthermore, the deep soil has more clay particles, a compact structure, and a more effective water conservation effect [30]. Because of the growth and coverage of *H. ammodendron*, the soil moisture content of the vegetation patches was significantly higher than that of the bare land patches [47]. The soil water content of the vegetation patches decreased at a depth of 100–150 cm (Figure 13), which was because the roots of *H. ammodendron* were mainly concentrated in the 50–150 cm soil layer away from the surface, and the roots absorbed the water needed for plant growth, which reduced the soil water content near the roots [48]. The root system absorbs water for plant growth, so the vegetation patch's soil moisture content was significantly higher than that of the bare

land patch [47]. The *H. ammodendron* plant had the highest humidity, gradually reducing to the periphery and forming a "wet island" centered on *H. ammodendron*, which shows that water is an important cause of patch formation patterns. This phenomenon indicated that *H. ammodendron* has a substantial self-collecting property [49].

The total salt content of the vegetation and bare land patches showed a "positive s" curve. That is, the soil salt content decreased first and then increased with the increase in soil depth (Figure 13). The high salt content at the soil surface is due to groundwater evaporation caused by high desert temperatures, and the salt is enriched in the soil surface [50]. The soil salt content of the vegetation patch was smaller than that of the bare land patch, and the lowest point of the *H. ammodendron* plants gradually increased towards the surrounding area, forming a "low salt area" centered on *H. ammodendron* [25,51]. The soil salt content of the vegetation patch was smaller than that of the bare land patch. The sudden increase point of the vegetation patch's soil salt content had a pre-phenomenon, which showed that *H. ammodendron* roots have an individual storage capacity for groundwater. The stem flow of salt-tolerant vegetation, such as *H. ammodendron* can take away the salt and reduce the salt content of the soil, which is also why the white crystals on the surface of the soil *H. ammodendron* [52]. Soil electrical conductivity as affected by soil moisture content and soil salt content. The vegetation and bare land patches' soil electrical conductivity showed a noticeable "inverted s" curve. According to the theory of "salt comes with water, salt goes with water" combined with the soil moisture content, and it can be inferred that the soil electrical conductivity of the vegetation patch was greatly affected by the water content [50] (Figure 13). However, the soil water content in the bare land patch increased as the soil depth increased; therefore, we speculated that soil salt content's influence on soil conductivity plays a significant role.

4.2. Changes of Soil Ions and Hydrochemical Types

The soil salt content of the vegetation patch increased obviously between May and October, but the salt secretion of *H. ammodendron* can reduce the soil salt content [53]. The bare land patches' soil salt content tended to be stable, and there was no significant change over time. The relationship between the total salt and anion content in the vegetation and bare land patches was similar. The soil total salt content had a strong correlation with SO_4^{2-}, followed by Cl^-, and had little correlation with HCO_3^-. SO_4^{2-} and Cl^- are the main anions in the eight major ions of soil, and the content of SO_4^{2-} and Cl^- is higher in the deep layer of soil. This is due to the intense evaporation in arid areas, the low water content in the surface soil, and the difficulty of decomposing the salt compounds, which is also why the high salt content in the surface soil of arid areas [54]. The ion with the lowest content in the soil was HCO_3^-, because HCO_3^- is mainly derived from the hydrolysis reaction of CO_2 in the oasis-desert ecotone, which results from less soil moisture [55]. Therefore, sulfates and chlorides are the main salts, with sulfates being the primary salt, in the oasis-desert ecotone soil in the Manas River Basin [56]. The correlation between the total soil salt and Ca^{2+} was strong, followed by Na^+, but there was no correlation with K^+ and Mg^{2+}. The main cations in the soil were Ca^{2+} and Na^+. Ca^{2+} first decreased and then increased with an increase in soil depth, which showed distinct distribution characteristics of shallow set surface aggregation [57]. The migration of Na^+ gradually increased with the increase in soil depth due to the soil colloid's effect on Na^+ [58]. The adsorption capacity of Na^+ is greater than that of Ca^{2+}, which caused the accumulation of Ca^{2+} at the soil surface as the water evaporated [59]. Ca^{2+} and Na^+ showed opposite trends in the process of soil salt conversion [60]. As sodium was the primary replacement, calcium salt decreased, and sodium gradually increased.

Comparing the hydrochemical types of the bare land and vegetation patches, we found that the Na^+ equivalent in VP was less than that in BP, which indicated that the root system of *H. ammodendron* could absorb sodium salt [61]. Some studies have pointed out white crystals on the surface of *H. ammodendron*. The roots of *H. ammodendron* absorb sodium salt for plant growth and development [57]. The sodium salt is extracted to the stem through

the roots of *H. ammodendron* and then separated from the leaves of *H. ammodendron* [62]. Sodium chloride is an essential index of secondary salinization in soil. *H. ammodendron* vegetation can reduce the secondary soil salinization [63]. In conclusion, the stability of *H. ammodendron* patch patterns in the oasis-desert ecotone in the southern margin of Junggar Basin is the result of the interaction between *H. ammodendron* vegetation and the arid environment.

4.3. Analysis of Water Sources and Utilization of H. ammodendron

Generally speaking, the stable isotope values of groundwater barely fluctuate with time and are relatively stable, which is due to the weakening of seasonal variation characteristics of precipitation in groundwater recharge through soil pore infiltration [64]. The $\delta^{18}O$ value of the soil water in the 0–100 cm shallow soil was significantly greater than that in the deep soil [65]. This was due to the fractionation of isotopes in water migration or phase transformation [66]. Under the influence of evaporation, water molecules composed of lighter isotopes in shallow soil water will preferentially evaporate into the air, which causes the heavy isotopes to become enriched in the shallow layer and increase the $\delta^{18}O$ value [67]. Before the rain, the primary water use source of *H. ammodendron* was groundwater, followed by soil water in the 120–180 cm soil layer. The water use efficiency of *H. ammodendron* for shallow soil was low; after rain, the primary water use source of *H. ammodendron* was the 60–120 cm soil layer, followed by groundwater. The main reason for this is that soil moisture content is small before rain, evaporation is extensive, and the shallow soil water absorption capacity of *H. ammodendron* is small and mainly relies on the central root system to absorb groundwater and deeper (>1.2 m) soil water to maintain growth [68]. After the rain, because precipitation cannot penetrate groundwater in a short time, it is instead found in the shallow soil layer, so *H. ammodendron* soil water use occurs in the shallow soil layer after rain ($\leq$1.2 m) [69].

H. ammodendron had a robust environmental adaptability for water uptake [70]. Due to the climate environment of high temperature and little rainfall in the desert, the water content of the soil surface was low, which inhibited the root activity of *H. ammodendron* [55]. The *H. ammodendron* root system tends to fishtail like a branch structure and has a robust spatial expansion ability [48]; the vertical root system is developed to obtain the groundwater over a larger space [71]. When there is rainfall supply, *H. ammodendron* can fully mobilise the shallow roots to absorb shallow soil water for growth. The adaptability of *H. ammodendron* to the environment was reflected in its soil water absorption and its consumption of water, and the liquid flow rate of *H. ammodendron* [5]. Specifically, the liquid flow rate of *H. ammodendron* appears to be in a temporary dormancy state when the solar radiation is the highest at noon, which is called a "noon break" [44,72]. This is because the solar radiation is too intense at noon, and the vegetation closes the stomata to reduce evaporation [47]. The difference between the daytime and night-time sap flow density of *H. ammodendron* increased with the decrease in soil salt content. The diurnal variation of the soil water content indicated that the root system of *H. ammodendron* had a reverse hydraulic lifting effect [53]. After precipitation, the utilisation ratio of *H. ammodendron* to the surface and deep groundwater increased. However, the ratio to the middle soil water decreased, and the "photosynthetic noon break" of the leaves was strong, which indicated that the root system of *H. ammodendron* had the function of hydraulic transmission [73]. The water redistribution of the *H. ammodendron* root system can maintain the balanced distribution of soil water, reduce the stress of the arid climate on *Haloxylon* vegetation, and improve the survivability of *Haloxylon* vegetation in the arid environment, which is also the fundamental reason for the formation and stability of *Haloxylon* vegetation patch patterns in the oasis-desert ecotone.

5. Conclusions

A "cold island", "wet island," and "low-salt" area formed that were centered around the *H. ammodendron* in VP. Soil water content in VP presented a reversed "S" type curve,

while BP's soil salinity presented an "S" type curve. NaCl was the most abundant in the BP soil, and the milligram equivalent of Cl^- was 80–90%, while $CaSO_4$ was the most abundant in the VP soil, in which the milligram equivalent of SO_4^{2-} was 80–100%. *H. ammodendron* has a robust environmental adaptability for water absorption and consumption. Before the rainfall, the contribution rate of each potential water source to *H. ammodendron* was groundwater > soil water (120–180 cm) > soil water (60–120 cm). After the rainfall, the contribution rate of each potential water source to *H. ammodendron* was soil water (0–60 cm) > soil water (60–120 cm) > groundwater.

Author Contributions: Conceptualisation, L.Z. and G.Y.; methodology, X.H.; software, W.L.; validation, L.Z., W.L. and G.Y.; formal analysis, L.T.; investigation, F.L.; resources, Y.G.; data curation, W.L.; writing—original draft preparation, L.Z. and W.L.; visualisation, K.Y.; supervision, X.H.; project administration, G.Y.; funding acquisition, X.H. All authors read and agreed to the published version of the manuscript.

Funding: This research was funded by the National Natural Science Foundation of China (grant number U1803244, 41761064); Key Technologies Research and Development Program (grant number 2017YFC0404303); Xinjiang Production and Construction Corps (grant numbers 2018CB023, CZ027204, 2018AB027, 2018BC007, 2019ZH13); and Shihezi University (grant number CXRC201801, RCZK2018C22).

Institutional Review Board Statement: Ethical review and approval were waived for this study, due to REASON. Not applicable" for studies not involving humans or animals.

Informed Consent Statement: Not applicable" for studies not involving humans.

Data Availability Statement: *H. ammodendron* plants were used in this study. *H. ammodendron* selected from 'Manas River Basin' (Wild plant, Shihezi, China) were kindly provided by Dr. Guang Yang (Xinjiang Production and Construction Group Key Laboratory of Modern Water-Saving Irrigation, Shihezi 832000, China).

Acknowledgments: The work was also supported by the Talent Program of Xinjiang Production and Construction Corps and Xinjiang Production and Construction Group Key Laboratory of Modern Water-Saving Irrigation.

Conflicts of Interest: The authors declare no conflict of interest.

References

1. Dunkerley, D.L. Banded vegetation: Development under uniform rainfall from a simple cellular automaton model. *Plant Ecol.* **1997**, *129*, 103–111. [CrossRef]
2. Pérez-Barbería, F.; Ramsay, S.; Hooper, R.; Pérez-Fernández, E.; Robertson, A.; Aldezabal, A.; Goddard, P.; Gordon, I. The influence of habitat on body size and tooth wear in Scottish red deer (Cervus elaphus). *Can. J. Zool.* **2015**, *93*, 61–70. [CrossRef]
3. Paschalis, A.; Katul, G.G.; Fatichi, S.; Manoli, G.; Molnar, P. Matching ecohydrological processes and scales of banded vegetation patterns in semiarid catchments. *Water Resour. Res.* **2016**, *52*, 2259–2278. [CrossRef]
4. Wang, G.H.; Zhao, W.Z.; Liu, H.; Zhang, G.F.; Li, F. Changes in soil and vegetation with stabilization of dunes in a desert-oasis ecotone. *Ecol. Res.* **2015**, *30*, 639–650. [CrossRef]
5. Gu, D.X.; Wang, Q.; Otieno, D. Canopy Transpiration and Stomatal Responses to Prolonged Drought by a Dominant Desert Species in Central Asia. *Water* **2017**, *9*, 404. [CrossRef]
6. Li, C.J.; Shi, X.; Lei, J.Q.; Xu, X.W. The scale effect on the soil spatial heterogeneity of Haloxylon ammodendron (C. A. Mey.) in a sandy desert. *Environ. Earth Sci.* **2014**, *71*, 4199–4207. [CrossRef]
7. Yang, G.; He, X.; Zhao, C.; Xue, L.; Chen, J. A saline water irrigation experimental investigation into salt-tolerant and suitable salt concentration of Haloxylon ammodendron from the Gurbantünggüt Desert, Northwestern China. *Fresen Environ. Bull* **2016**, *25*, 3408–3416.
8. Wang, L.; Cai, Q.; Cai, C.; Sun, L. Morphological changes of rill on loess slope and its relationship with flow velocity. *Trans. Chin. Soc. Agric. Eng.* **2014**, *30*, 110–117. [CrossRef]
9. Itoh, A.; Yamakura, T.; Ohkubo, T.; Kanzaki, M.; Palmiotto, P.A.; LaFrankie, J.V.; Ashton, P.S.; Lee, H.S. Importance of topography and soil texture in the spatial distribution of two sympatric dipterocarp trees in a Bornean rainforest. *Ecol. Res.* **2003**, *18*, 307–320. [CrossRef]
10. Enoki, T.; Kawaguchi, H.; Iwatsubo, G. Topographic variations of soil properties and stand structure in a Pinus thunbergii plantation. *Ecol. Res.* **1996**, *11*, 299–309. [CrossRef]

11. Chen, Y.; Yu, F.; Dong, M. Spatial heterogeneity of the psammophytic half-shrub community in Mu Us Sandland. *Acta Ecol. Sin.* **2000**, *20*, 568–572. [CrossRef]
12. Yang, G.; Li, F.; Chen, D.; He, X.; Xue, L.; Long, A. Assessment of changes in oasis scale and water management in the arid Manas River Basin, north western China. *Sci. Total Environ.* **2019**, *691*, 506–515. [CrossRef]
13. Liu, Z.; Liu, T.; Zhang, R.; CHENG, H.-h. Species diversity and spatial differentiation of ephemeral plant community in southern Gurbantunggut Desert. *Chin. J. Ecol.* **2011**, *30*, 45–52. [CrossRef]
14. Sheffer, E.; Yizhaq, H.; Shachak, M.; Meron, E. Mechanisms of vegetation-ring formation in water-limited systems. *J. Theor. Biol.* **2011**, *273*, 138–146. [CrossRef]
15. Oddi, F.; Ghermandi, L.; Lasaponara, R. Dendroecological potential of Fabiana imbricata shrub for reconstructing fire history at landscape scale in grasslands. In Proceedings of the EGU General Assembly Conference Abstracts, Vienna, Austria, 8–13 April 2018.
16. Meinzer, F.C.; Andrade, J.L.; Goldstein, G.; Holbrook, N.M.; Cavelier, J.; Wright, S.J. Partitioning of soil water among canopy trees in a seasonally dry tropical forest. *Oecologia* **1999**, *121*, 293–301. [CrossRef]
17. Yang, G.; Li, F.; Tian, L.; He, X.; Gao, Y.; Wang, Z.; Ren, F. Soil physicochemical properties and cotton (Gossypium hirsutum L.) yield under brackish water mulched drip irrigation. *Soil Tillage Res.* **2020**, *199*, 104592. [CrossRef]
18. Dawson, L.; Duff, E.; Campbell, C.; Hirst, D. Depth distribution of cherry (Prunus avium L.) tree roots as influenced by grass root competition. *Plant Soil* **2001**, *231*, 11–19. [CrossRef]
19. Zhang, T.; Li, Z.; Li, P.; Xu, G.; Liu, X.; Jin, Y. Response characteristics of soil water use patterns by different plants to precipitation in rocky mountainou areas. *J. Appl. Ecol.* **2016**, *27*, 1461–1467. [CrossRef]
20. Lin, G.; Da S.L. Sternberg, L. Hydrogen isotopic fractionation by plant roots during water uptake in coastal wetland plants. In *Stable Isotopes and Plant Carbon-Water Relations*; Elsevier: Amsterdam, The Netherlands, 1993; pp. 497–510. [CrossRef]
21. Zhou, H.; Zhao, W.; Zhang, G. Varying water utilization of Haloxylon ammodendron plantations in a desert-oasis ecotone. *Hydrol. Process.* **2017**, *31*, 825. [CrossRef]
22. Song, L.; Jin, J.; He, J. Effects of Severe Water Stress on Maize Growth Processes in the Field. *Sustainability* **2019**, *11*, 5086. [CrossRef]
23. Aguiar, M.; Sala, O.E. Patch structure, dynamics and implications for the functioning of arid ecosystems. *Trends Ecol. Evol.* **1999**, *14*, 273–277. [CrossRef]
24. Li, J.; Zhao, C.; Zhu, H.; Li, Y.; Wang, F. Effect of plant species on shrub fertile island at an oasis-desert ecotone in the South Junggar Basin, China. *J. Arid Environ.* **2007**, *71*, 350–361. [CrossRef]
25. Wang, Y.G.; Li, Y.; Xiao, D.N. Catchment scale spatial variability of soil salt content in agricultural oasis, Northwest China. *Environ. Geol.* **2008**, *56*, 439–446. [CrossRef]
26. Xu, L.; Du, H.; Zhang, X. Spatial Distribution Characteristics of Soil Salinity and Moisture and Its Influence on Agricultural Irrigation in the Ili River Valley, China. *Sustainability* **2019**, *11*, 7142. [CrossRef]
27. Kéfi, S.; Rietkerk, M.; Alados, C.L.; Pueyo, Y.; Papanastasis, V.P.; ElAich, A.; Ruiter, P.C.d. Spatial vegetation patterns and imminent desertification in Mediterranean arid ecosystems. *Nat. Int. Wkly. J. Sci.* **2007**, *449*, 213–217. [CrossRef]
28. Ludwig, J.A.; Wilcox, B.P.; Breshears, D.D.; Tongway, D.J.; Imeson, A.C. Vegetation Patches And Runoff–Erosion As Interacting Ecohydrological Processes In Semiarid Landscapes. *Ecology* **2005**, *86*, 225–236. [CrossRef]
29. Luo, W.; Zhao, W.; He, Z.; Sun, C. Spatial characteristics of two dominant shrub populations in the transition zone between oasis and desert in the Heihe River Basin, China. *Catena* **2018**, *170*, 356–364. [CrossRef]
30. Xu, G.Q.; Li, Y.; Xu, H. Seasonal variation in plant hydraulic traits of two co-occurring desert shrubs, Tamarix ramosissima and Haloxylon ammodendron, with different rooting patterns. *Ecol. Res.* **2011**, *26*, 1071–1080. [CrossRef]
31. Li, X.; Zhang, Z.; Huang, L.; Wang, X. Review of the ecohydrological processes and feedback mechanisms controlling sand-binding vegetation systems in sandy desert regions of China. *Chin. Sci. Bull.* **2013**, *58*, 1483–1496. [CrossRef]
32. Ke, Z.; Yongzhong, S.; Ting, W.; Tingna, L. Soil properties and herbaceous characteristics in an age sequence of Haloxylon ammodendron plantations in an oasis-desert ecotone of northwestern China. *J. Arid Land* **2016**, *8*, 960–972. [CrossRef]
33. Peng, N.Y.; Song, C.H.; Ke-Lin, W.; Susanne, S. Challenges and probable solutions for using stable isotope techniques to identify plant water sources in karst regions: A review. In *J. Appl. Ecol.*; 2017; 28, pp. 2361–2368. [CrossRef]
34. Stromberg, J.; Patten, D. Instream flow and cottonwood growth in the eastern Sierra Nevada of California, USA. *Rivers Res. Appl.* **1996**, *12*, 1–12. [CrossRef]
35. Phillips, D.L.; Gregg, J.W. Source partitioning using stable isotopes: Coping with too many sources. *Oecologia* **2003**, *136*, 261–269. [CrossRef] [PubMed]
36. Zhao, Z.-m.; Shi, F.-x. Contribution of root respiration to spatial-temporal variation of soil respiration in a Haloxylon ammodendrons ecosystem in Gurbantunggut Basin. *Acta Ecol. Sin.* **2017**, *37*, 392–398. [CrossRef]
37. Cecil, R.; McPhee, J. The estimation of thiols and disulphides by potentiometric titration with silver nitrate. *Biochem. J.* **1955**, *59*, 234. [CrossRef]
38. Flaschka, H.A. *EDTA Titrations: An Introduction to Theory and Practice*; Elsevier: Amsterdam, The Netherlands, 2013; Volume 106, p. 8. [CrossRef]
39. Mehta, S.A.; Bonakdarpour, A.; Wilkinson, D.P. Impact of cathode additives on the cycling performance of rechargeable alkaline manganese dioxide–zinc batteries for energy storage applications. *J. Appl. Electrochem.* **2017**, *47*, 167–181. [CrossRef]

40. Barnes, R.B.; Richardson, D.; Berry, J.W.; Hood, R.L. Flame photometry a rapid analytical procedure. *Ind. Eng. Chem. Anal. Ed.* **1945**, *17*, 605–611. [CrossRef]
41. Abbaspour, A.; Kamyabi, M.; Khalafi-Nezhad, A.; Soltani Rad, M. Acidity constants and thermodynamic parameters of some phenol derivatives in methanol+ water systems using potentiometry and spectrophotometry methods. *J. Chem. Eng. Data* **2003**, *48*, 911–915. [CrossRef]
42. Phillips, D.L.; Gregg, J.W. Uncertainty in source partitioning using stable isotopes. *Oecologia* **2001**, *127*, 171–179. [CrossRef]
43. Qiu, G.Y.; Li, C.; Yan, C. Characteristics of soil evaporation, plant transpiration and water budget of Nitraria dune in the arid Northwest China. *Agric. For. Meteorol.* **2015**, *203*, 107–117. [CrossRef]
44. Zheng, C.; Wang, Q. Seasonal and annual variation in transpiration of a dominant desert species, Haloxylon ammodendron, in Central Asia up-scaled from sap flow measurement. *Ecohydrology* **2015**, *8*, 268. [CrossRef]
45. Ao, Y.H.; Lyu, S.H.; Han, B.; Li, Z.G. Comparative analysis of the soil thermal regimes of typical underlying surfaces of oasis systems in an Arid Region. *Environ. Earth Sci.* **2015**, *73*, 7889–7896. [CrossRef]
46. Cao, X.M.; Wang, J.L.; Chen, X.; Gao, Z.Q.; Yang, F.; Shi, J.K. Multiscale remote-sensing retrieval in the evapotranspiration of Haloxylon ammodendron in the Gurbantunggut desert, China. *Environ. Earth Sci.* **2013**, *69*, 1549–1558. [CrossRef]
47. Yang, Y.; Zhou, H.; Xu, L. Dynamic variations of soil moisture in Haloxylon ammodendron root zone in Gurbantunggut Desert. *J. Appl. Ecol.* **2011**, *22*, 1711–1716. [CrossRef]
48. Zhou, H.; Zhao, W.; Yang, Q. Root biomass distribution of planted Haloxylon ammodendron in a duplex soil in an oasis: Desert boundary area. *Ecol. Res.* **2016**, *31*, 598. [CrossRef]
49. Nian, W.; Guo, J.; Zhang, J.; Fang, J. Effects of nanosecond pulsed electric field exposure on seed of Saxaul (Haloxylon ammodendron). In Proceedings of the 2013 Abstracts IEEE International Conference on Plasma Science (ICOPS), San Francisco, CA, USA, 16–21 June 2013; p. 1-1.
50. Gu, F.X.; Chu, Y.; Zhang, Y.D.; Liu, Y.Q.; Anabiek, S.; Ye, Q.; Pan, X.L. Spatial and temporal dynamics of soil moisture and salinity in typical plant communities of Sangonghe Basin. In *Ecosystems Dynamics, Ecosystem-Society Interactions, And Remote Sensing Applications for Semi-Arid And Arid Land, Pts 1 And 2*; Pan, X.L., Gao, W., Glantz, M.H., Honda, Y., Eds.; Spie-Int Soc Optical Engineering: Bellingham, WA, USA, 2003; Volume 4890, pp. 471–479. [CrossRef]
51. Lilong, W.; Guanxiang, Z.; Meng, L.; Mingting, Z.; Lifang, Z.; Xinfang, Z.; Lizhe, A.; Shijian, X. C:N:P stoichiometry and leaf traits of halophytes in an arid saline environment, northwest China. *PLoS ONE* **2015**, 10. [CrossRef]
52. Xingming, H.; Weihong, L. Oasis cold island effect and its influence on air temperature: A case study of Tarim Basin, Northwest China. *J. Arid Land* **2016**, *8*, 172–183. [CrossRef]
53. Maina, J.N.; Wang, Q. Seasonal Response of Chlorophyll a/b Ratio to Stress in a Typical Desert Species: Haloxylon ammodendron. *Arid Land Res. Manag.* **2015**, *29*, 321–334. [CrossRef]
54. Su, Y.Z.; Wang, X.F.; Yang, R.; Yang, X.; Liu, W.J. Soil Fertility, Salinity and Nematode Diversity Influenced by Tamarix ramosissima in Different Habitats in an Arid Desert Oasis. *Environ. Manag.* **2012**, *50*, 226–236. [CrossRef]
55. Yang, W.B.; Feng, W.; Jia, Z.Q.; Zhu, Y.J.; Guo, J.Y. Soil water threshold for the growth of Haloxylon ammodendron in the Ulan Buh desert in arid northwest China. *S. Afr. J. Bot.* **2014**, *92*, 53–58. [CrossRef]
56. Arndt, S.K.; Arampatsis, C.; Foetzki, A.; Li, X.Y.; Zeng, F.J.; Zhang, X.M. Contrasting patterns of leaf solute accumulation and salt adaptation in four phreatophytic desert plants in a hyperarid desert with saline groundwater. *J. Arid Environ.* **2004**, *59*, 259–270. [CrossRef]
57. Wang, S.M.; Wan, C.G.; Wang, Y.R.; Chen, H.; Zhou, Z.Y.; Fu, H.; Sosebee, R.E. The characteristics of Na+, K+ and free proline distribution in several drought-resistant plants of the Alxa Desert, China. *J. Arid Environ.* **2004**, *56*, 525–539. [CrossRef]
58. Kang, J.J.; Duan, J.J.; Wang, S.M.; Zhao, M.; Yang, Z.H. Na compound fertilizer promotes growth and enhances drought resistance of the succulent xerophyte Haloxylon ammodendron. *Soil Sci. Plant Nutr.* **2013**, *59*, 289–299. [CrossRef]
59. Dong, X.J.; Zhang, X.S. Some observations of the adaptations of sandy shrubs to the arid environment in the Mu Us Sandland: Leaf water relations and anatomic features. *J. Arid Environ.* **2001**, *48*, 41–48. [CrossRef]
60. Kang, J.; Zhao, W.; Su, P.; Zhao, M.; Yang, Z. Sodium (Na^+) and silicon (Si) coexistence promotes growth and enhances drought resistance of the succulent xerophyte Haloxylon ammodendron. *Soil Sci. Plant Nutr.* **2014**, *60*, 659–669. [CrossRef]
61. Gu, F.X.; Zhang, Y.D.; Pan, X.L.; Chu, Y.; Shi, Q.D.; Ye, Q. Effects of spatial and temporal dynamics of soil water and salinity on new oasis stability. In *Ecosystems Dynamics, Ecosystem-Society Interactions, And Remote Sensing Applications for Semi-Arid And Arid Land, Pts 1 And 2*; Pan, X.L., Gao, W., Glantz, M.H., Honda, Y., Eds.; Spie-Int Soc Optical Engineering: Bellingham, WA, USA, 2003; Volume 4890, pp. 128–140. [CrossRef]
62. Su, Y.; Liu, T.; Kong, J. The establishment and development of Haloxylon ammodendron promotes salt accumulation in surface soil of arid sandy land. *Sci. Cold Arid Reg.* **2019**, *11*, 116–125.
63. Li, C.J.; Li, Y.; Ma, J.; Fan, L.L.; Wang, Q.X. Spatial heterogeneity of soil chemical properties between Haloxylon persicum and Haloxylon ammodendron populations. *J. Arid Land* **2010**, *2*, 257–265. [CrossRef]
64. Gries, D.; Zeng, F.; Foetzki, A.; Arndt, S.K.; Bruelheide, H.; Thomas, F.M.; Zhang, X.; Runge, M. Growth and water relations of Tamarix ramosissima and Populus euphratica on Taklamakan desert dunes in relation to depth to a permanent water table. *Plant Cell Environ.* **2003**, *26*, 725–736. [CrossRef]
65. Dai, Y.; Zheng, X.J.; Tang, L.S.; Li, Y. Stable oxygen isotopes reveal distinct water use patterns of two Haloxylon species in the Gurbantonggut Desert. *Plant Soil* **2015**, *389*, 73–87. [CrossRef]

66. Brunel, J.P.; Walker, G.R.; Kennettsmith, A.K. Field Validation Of Isotopic Procedures For Determining Sources Of Water Used By Plants In A Semiarid Environment. *J. Hydrol.* **1995**, *167*, 351–368. [CrossRef]
67. Walker, C.D.; Richardson, S.B. The use of stable isotopes of water in characterising the source of water in vegetation. *Elsevier* **1991**, *94*, 145–158. [CrossRef]
68. Li, B.; Han, Z.; Hu, H.; Bai, C. Study on the effect of groundwater flow on the identification of thermal properties of soils. *Renew. Energy* **2020**, *147*, 2688–2695. [CrossRef]
69. Shan, L.S.; Zhang, X.M.; Wang, Y.K.; Wang, H.; Yan, H.N.; Wei, J.; Xu, H. Influence of moisture on the growth and biomass allocation in Haloxylon ammodendron and Tamarix ramosissima seedlings in the shelterbelt along the Tarim Desert Highway, Xinjiang, China. *Chin. Sci. Bull.* **2008**, *53*, 93–101. [CrossRef]
70. Li, C.J.; Li, Y.; Ma, J.A. Spatial heterogeneity of soil chemical properties at fine scales induced by Haloxylon ammodendron (Chenopodiaceae) plants in a sandy desert. *Ecol. Res.* **2011**, *26*, 385–394. [CrossRef]
71. Yu, T.; Ren, C.; Zhang, J.; He, X.; Ma, L.; Chen, Q.; Qu, Y.; Shi, S.; Zhang, H.; Ma, H. Effect of high desert surface layer temperature stress on Haloxylon ammodendron (C.A. Mey.) Bunge. *Flora* **2012**, *207*, 572–580. [CrossRef]
72. Gu, D.X.; Wang, Q.; Mallik, A. Non-convergent transpiration and stomatal conductance response of a dominant desert species in central Asia to climate drivers at leaf, branch and whole plant scales. *J. Agric. Meteorol.* **2018**, *74*, 9–17. [CrossRef]
73. Wu, X.; Zheng, X.J.; Yin, X.W.; Yue, Y.M.; Liu, R.; Xu, G.Q.; Li, Y. Seasonal variation in the groundwater dependency of two dominant woody species in a desert region of Central Asia. *Plant Soil* **2019**, *444*, 39–55. [CrossRef]